第 43 卷 第 1 期/2023 年 1 月/光学学报 研究论文

光学学报

可调谐垂直腔面发射激光器支撑结构优化设计

吕家纲[1,2]，李伟[1*]，戚宇轩[1,2]，潘智鹏[1,2]，仲莉[1]，刘素平[1]，马骁宇[1]

[1]中国科学院半导体研究所光电子器件国家工程研究中心，北京 100083；

[2]中国科学院大学材料科学与光电技术学院，北京 100049

摘要 基于微机电系统(MEMS)的850 nm可调谐垂直腔面发射激光器(VCSEL)，设计了一种双曲线梁结构，以提升器件机械和调谐特性。通过分析传统等截面梁结构的受力情况，提出了双曲线结构优化设计，将梁结构端面的面积增大从而降低最大应力。理论仿真结果表明：优化后器件上反射镜的最大偏移量基本保持不变，支撑梁上下表面的最大应力分别降低了23.4%和17.0%，谐振频率增大了7.9%；当MEMS-VCSEL分别为半导体腔主导(SCD)结构和空气腔主导(ACD)结构时，波长调谐范围分别为16.6 nm和42 nm。该优化方式的优势在于不需要改变激光器的结构，同时可与其他优化方式兼容，具有一定的应用前景。

关键词 激光器；垂直腔面发射激光器；可调谐激光器；微机电系统；机械特性；调谐特性

中图分类号 TN365 **文献标志码** A **DOI**：10.3788/AOS221271

1 引 言

垂直腔面发射激光器(VCSEL)具有低阈值电流、低功耗、小发散角、动态单纵模、圆形光斑和易于二维集成等优点[1-3]，在工业加工、数据通信、光互连和固体激光泵浦等领域中得到了广泛的应用[4-6]。VCSEL常与微机电系统(MEMS)技术相结合，以实现波长可调谐的激光输出，具有宽连续波长调谐范围、快调谐速率和低功耗等优势。光通信[7-9]、光学相干层析成像[10-12]和激光雷达[13]等领域对光源的波长覆盖范围和扫频速率都有一定的要求，故MEMS-VCSEL在其中具有良好的应用前景。

1995年，MEMS-VCSEL在美国斯坦福大学被第一次提出并制备，在930 nm波段附近波长调谐范围达到15 nm[14]。2008年，Huang等[15]提出利用高对比度光栅替代传统VCSEL的分布式布拉格(DBR)反射镜，在850 nm波段实现了18 nm的波长调谐。随后各个研究小组在不同的波段采用不同的结构和调谐方式均取得了一定的突破，其研究目标是拓宽器件的调谐范围和提升器件的调谐速率[16-20]。在上述可调谐应用中，MEMS-VCSEL器件的悬浮反射镜均由等截面梁结构支撑，调谐过程中等截面梁结构会受到交变载荷，由此导致的结构断裂是限制MEMS结构寿命的主要因素之一[21-22]。

由于不同材料的力学性能存在一定的差异，故MEMS结构的可靠性很大程度上取决于使用的材料体系[23]。除了材料，器件的封装方式对其性能和可靠性也起着至关重要的作用，但引入额外的封装工艺会增加器件的工艺成本，这会限制其在商业应用上的发展[24]。除了材料体系和封装工艺，MEMS的结构也直接影响着器件的性能和可靠性[25]，对结构进行一定的优化设计可以在低成本条件下提高器件的可靠性，是一种可行性较高的优化方式。

本文对MEMS中支撑梁结构对可调谐VCSEL性能和可靠性的影响进行了研究。对传统等截面结构进行了力学分析，并提出了双曲线结构优化设计，以降低支撑梁结构上的最大应力，进而改善整体应力分布。在反射镜最大偏移量基本不变的情况下，所提结构中支撑梁上下表面应力分别降低了23.4%和17.0%，谐振频率提升了7.9%。该设计无需引入额外的工艺步骤即可提升器件的机械与调谐特性，且与其他材料、结构优化方式具有良好的兼容性。

2 优化设计

MEMS-VCSEL的整体结构如图1所示，器件包括半VCSEL部分、耦合层、空气隙和一个可偏移的上反射镜，其中：半VCSEL部分包含底部电极、衬底、下部DBR反射镜、有源区和氧化层；耦合层主要为中部DBR和电流注入层；器件中的空气隙是通过选择性湿法腐蚀制备的；上反射镜一般为DBR反射镜或亚波长

收稿日期：2022-06-07；**修回日期**：2022-07-02；**录用日期**：2022-07-11；**网络首发日期**：2022-07-21

基金项目：国家自然科学基金(62174154)

通信作者：*liwei66@semi.ac.cn

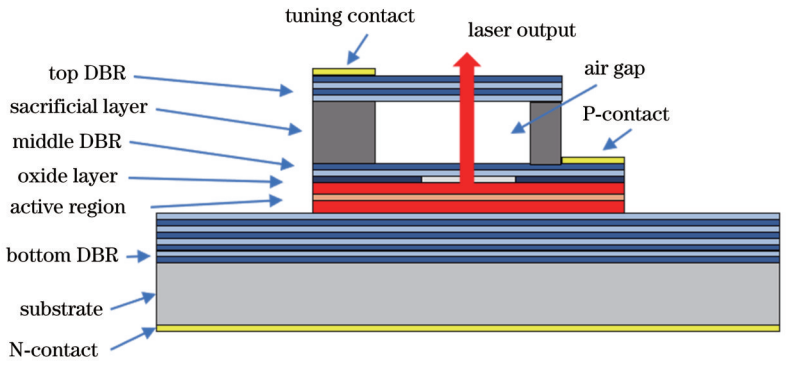

图 1　MEMS-VCSEL结构示意图

Fig. 1　Structural diagram of MEMS-VCSEL

高对比度光栅反射镜。

MEMS结构一般是通过材料的压阻、压电、静电、热敏或者电磁特性来驱动和传感的，其中静电驱动是MEMS-VCSEL中最常用的驱动方式。此时，MEMS部分在器件中相当于一个可变气隙电容，在顶部调谐电极和中部电流注入电极之间施加反向偏压，上反射镜就会受静电力的牵引向下偏移，空气隙厚度发生变化，从而器件的输出波长会发生改变[26]。当上反射镜受到静电力驱动时，上反射镜的支撑结构可以简化为受到一维均匀载荷的梁结构，此时其受到的剪切力和弯矩分布如图2所示，其中l为梁的长度，V为梁结构的剪切力分布，M_{max}为梁结构的最大弯矩。

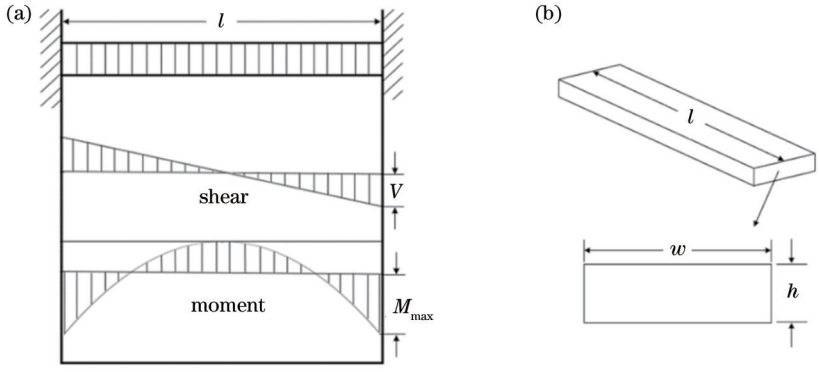

图 2　三维梁结构和受力分析。(a)简化梁结构受力分析；(b)梁结构的三维示意图

Fig. 2　Three-dimensional beam structure and stress analysis. (a) Stress analysis of simplified beam structure; (b) three-dimensional diagram of beam structure

可以看到，受到均匀载荷时剪切力和弯矩均在端面达到最大值，此时梁上的应力σ[27]可以表示为

$$\sigma=\frac{M}{S},\tag{1}$$

式中：M为弯矩；S为梁的截面模量，是与梁结构的截面几何尺寸相关联的参数。对于矩形截面，S[27]可表示为

$$S=\frac{w\cdot h^2}{6},\tag{2}$$

式中：w和h分别为梁结构截面的宽和高。

在MEMS中，支撑梁多为矩形等截面结构，故在梁的端面处容易出现应力集中现象。已有研究通过显微拉曼光谱测量得出，在静电驱动的可调谐VCSEL中，MEMS的端点处残余应力最大[28]。在工程力学中，可以通过改变梁结构的截面形貌（如采用“工”字梁）来降低应力，但微纳尺度下难以通过这种方式来优化梁结构的应力分布。然而，梁结构的截面尺寸是可以通过设计来改变的，由之前的分析可知，端面处弯矩最大，而截面模量不变，因此应力最大。本研究将传统等截面支撑梁优化为双曲线结构，优化前后梁的体积不变，通过增大两端面的截面尺寸，增大端面截面模量，从而降低端面位置的应力，使得支撑梁上最大应力降低，应力分布更均匀，图3为优化前后的结构示意图。

在图3所示的示意图中，中间的正方形结构为上反射镜，边长为C，两种梁的长度均为L。对于等截面结构，梁宽为W。对于双曲线结构，梁中部腰位置处的梁宽为$2a$，端面处的梁宽为$a\sqrt{4b^2+L^2}/b$，确定梁宽的双曲线方程为

$$\frac{x^2}{a^2}-\frac{y^2}{b^2}=1,\tag{3}$$

式中：(x,y)为双曲线梁结构上不同点的位置；a和b为双曲线的实半轴和虚半轴长。两种结构的材料参数

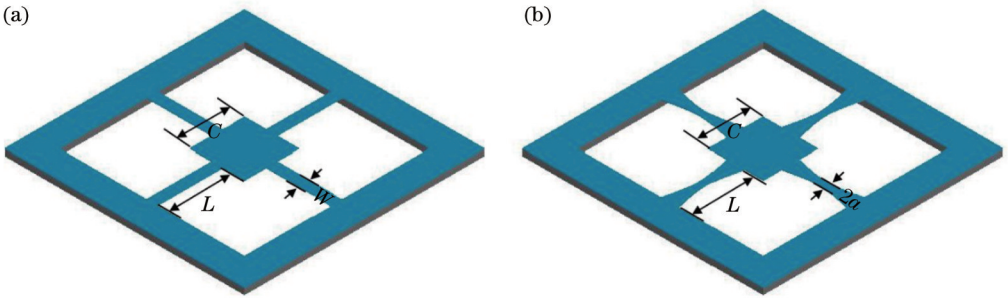

图 3 悬浮反射镜结构示意图。(a)等截面结构;(b)双曲线结构

Fig. 3 Structural diagram of suspended mirror. (a) Constant section structure; (b) hyperbolic structure

和几何参数如表 1 所示。

表 1 两种结构的材料参数和几何参数[29]

Table 1 Material and geometric parameters of two structures[29]

Parameter	Value
a in Eq. (3)	3
b in Eq. (3)	20.18
Width W /μm	10
Length L /μm	100
Thickness of mirror H /μm	2.8
Side length C /μm	40
Poisson radio	0.37
Young's modulus E /GPa	84.22
Density /(kg·m^{-3})	4384
Relative permittivity	11.20
Air gap thickness /μm	1.0625

3 分析与讨论

3.1 机械特性

对于两种结构,在相同的偏移量下,对比了两种结构的力学特性。图 4 为两种结构在偏移量为 390 nm 时,支撑梁上下表面的应力分布。可以看到,优化前后的应力分布相似,在两个端面应力值较大,而在梁的中间位置应力较小,表面应力最大值出现在固定端面附近,对于传统的等截面结构,上下表面的最大应力分别为 3.25×10^7 N/m^2 和 3.06×10^7 N/m^2,优化后双曲线结构上下表面的最大应力分别为 2.49×10^7 N/m^2 和 2.54×10^7 N/m^2,分别下降了 23.4% 和 17.0%。

图 5 为两种结构端面位置的应力分布,图 5(a)为传统等截面结构上下表面在端面位置的应力分布,图 5(b)为优化后双曲线结构上下表面在端面位置的应力分布。可以看出,两种结构端面位置应力分布类似,对于固定端面位置,在支撑梁的中部出现了应力集中现象,而对于连接端面位置,在支撑梁的两端点处出现了应力集中现象。在优化之后,由于双曲线结构端面宽度更大,截面模量更大,因此应力相较于传统等截面有所降低。

在已知双曲线结构能降低支撑梁上的最大应力后,对双曲线结构中梁的弯曲程度对结构机械特性的影响进行了分析,在参数 a 分别取值 1、2、3、4,且支撑梁体积不变时,计算了支撑梁的固定端面、连接端面和腰部截面位置的最大应力,结果如图 6 所示。随着参数 a 的增大,腰部截面的面积在增大,两端面的面积在减小,腰部截面的最大应力在降低,固定端面和连接端面的最大应力在增大。当参数 a 由 3 增大到 4 时,两端面的最大应力迅速增大,而腰部截面的最大应力下降

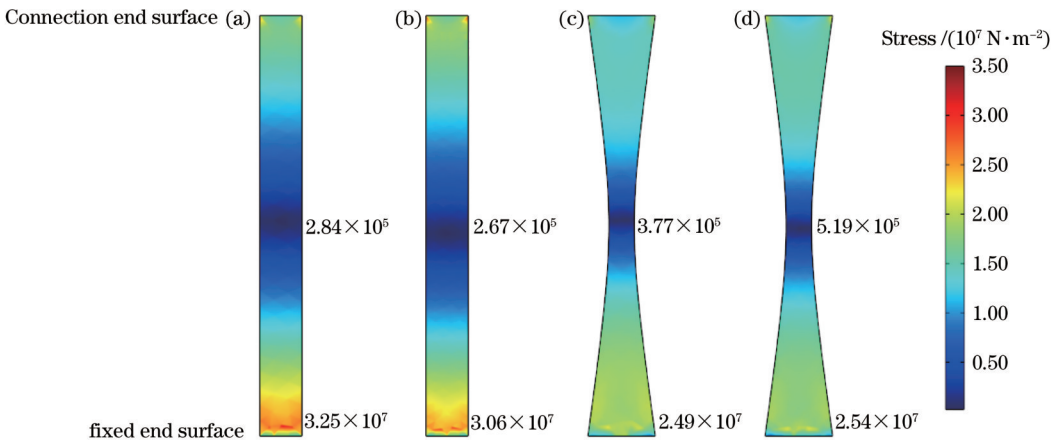

图 4 梁结构的应力分布。(a)等截面结构的上表面;(b) 等截面结构的下表面;(c)双曲线结构的上表面;(d)双曲线结构的下表面

Fig. 4 Stress distribution for beam structure. (a) Upper surface of constant section structure; (b) lower surface of constant section structure; (c) upper surface of hyperbolic structure; (d) lower surface of hyperbolic structure

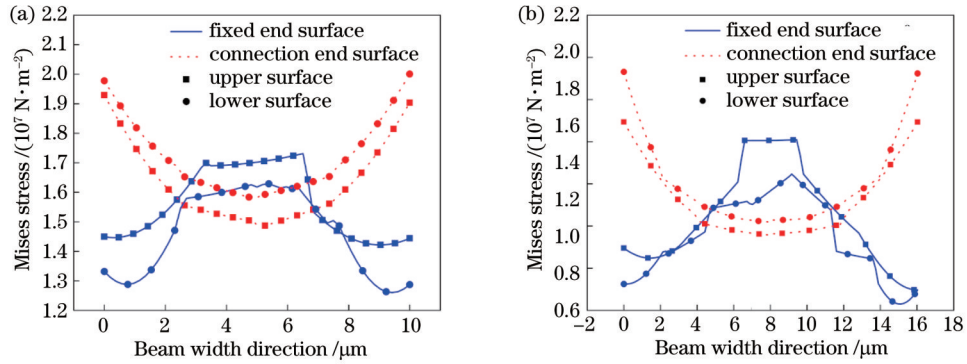

图 5　上下表面端面处的应力分布。(a)等截面结构;(b)双曲线结构

Fig. 5　Stress distribution on end surfaces of upper and lower surfaces. (a) Constant section structure; (b) hyperbolic structure

不明显,故当参数 a 为 3 时,整体结构的应力结果比较合适。

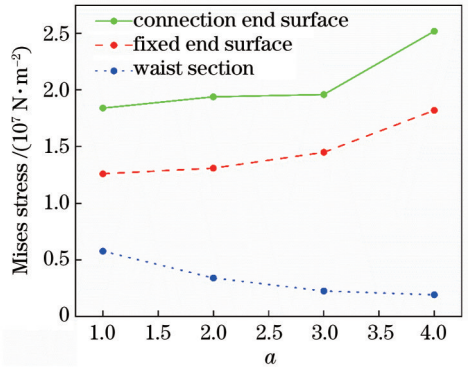

图 6　不同 a 时两端面和腰部截面的最大应力

Fig. 6　Maximum stress of two end surfaces and waist section under different a

在静电驱动 MEMS-VCSEL 中,顶部反射镜的偏移量主要由静电力和材料的弹性恢复力共同决定。当两者达到平衡状态时,反射镜会达到偏移的临界状态,继续增大上反射镜上的反向偏压会导致静电力与弹性恢复力失衡,从而使得上反射镜迅速向下偏移直至与下方结构贴合,该现象被称为“吸合现象”[30]。“吸合现象”发生时的反向偏压被称为“吸合偏压”,对应的偏移量为上反射镜的最大偏移量(被称为“吸合位移”),静电驱动 MEMS-VCSEL 的“吸合位移”一般约为空气隙大小的 1/3。表 2 为传统等截面结构和参数 a 不同时双曲线结构的“吸合位移”与“吸合偏压”。可以看到:传统等截面结构上反射镜的最大偏移量约为 402.5 nm,对应的反向偏压约为 28.79 V;对于双曲线结构,随着参数 a 的增大,结构上反射镜的最大偏移量有所增大,对应的反向偏压略有降低,这是由结构的弹性系数略微降低导致的;当参数 a 取值为 3 或 4 时,双曲线结构上反射镜的最大偏移量与传统等截面结构相差不大,对应的“吸合偏压”略有增加。

表 2　两种结构不同参数下的“吸合”位移与电压

Table 2　"Pull-in" displacements and voltages of two structures under different parameters

Structure	"Pull-in" displacement / nm	"Pull-in" voltage /V
Constant section structure	402.5	28.79
Hyperbolic structure (a=1)	386.5	31.95
Hyperbolic structure (a=2)	389.5	31.72
Hyperbolic structure (a=3)	393.5	31.24
Hyperbolic structure (a=4)	397.5	30.29

3.2　调谐特性

对于 MEMS-VCSEL,波长调谐范围是衡量器件的重要指标之一,一般由器件上反射镜的最大偏移量、器件的最小自由光谱范围(FSR),以及反射镜的高反射带宽和增益谱宽共同决定[31]。针对 850 nm 波长的 MEMS-VCSEL,设计了如表 3 所示的激光器结构,并结合参数 a 取值为 3 时上反射镜的最大偏移量计算了器件的波长调谐范围。

表 3　MEMS-VCSEL 器件的结构参数[29, 32]

Table 3　Structural parameters of MEMS-VCSEL devices[29, 32]

Component	Material	Thickness /nm	Refractive index n
Top DBR (23 pairs)	$Al_{0.12}Ga_{0.88}As/Al_{0.9}Ga_{0.1}As$	59.8/69.4	3.5542/3.0136
Air cavity	Air	1062.5	1
Middle DBR (2 pairs)	$Al_{0.12}Ga_{0.88}As/Al_{0.9}Ga_{0.1}As$	59.8/69.4	3.5542/3.0136
Oxide layer	$Al_{0.98}Ga_{0.02}As$	30	3.0136
Active region	GaAs/AlGaAs	6/8	3.6550/3.4253
Bottom DBR (39.5 pairs)	$Al_{0.12}Ga_{0.88}As/Al_{0.9}Ga_{0.1}As$	59.8/69.4	3.5542/3.0136

可将 MEMS-VCSEL 视为一个由半导体腔与空气腔耦合而成的法布里-珀罗腔，其谐振条件为

$$\phi_{\text{total}}(\lambda)=2m\cdot\pi, \tag{4}$$

式中：m 为整数；λ 为波长；$\phi_{\text{total}}(\lambda)$ 为总相位，其[33]还可表示为

$$\phi_{\text{total}}(\lambda)=\phi_{\text{top}}(\lambda)+\phi_{\text{cavity+bottom}}(\lambda), \tag{5}$$

式中：$\phi_{\text{top}}(\lambda)$ 为顶部反射相位；$\phi_{\text{cavity+bottom}}(\lambda)$ 为包括半导体腔在内的底部反射相位。

在 MEMS-VCSEL 中，空气隙厚度会随着反射镜的偏移不断减小，此时上反射镜的反射率变化较小，但光进入上反射镜的相位发生了变化，整体腔的谐振波长因此也发生了变化。图 7 为 VCSEL 分别为半导体腔主导（SCD）结构和空气腔主导（ACD）结构时的光场分布：对于 SCD 结构，半导体腔与空气腔之间的耦合层表现为高反层，光场主要被限制在半导体腔中；对于 ACD 结构，半导体腔与空气腔之间的耦合层表现为增透层，光场主要被限制在空气腔中。因此，ACD 结构的空气隙变化对谐振波长的影响更大。图 8 为两种结构的谐振波长随外加反向偏压的变化结果。对于 SCD 结构，当外加偏压为 0 时，空气隙厚度为 1062.5 nm，此时器件的谐振波长为 860.6 nm。随着外加反向偏压的增大，上反射镜向下偏移，空气隙厚度降低，器件谐振波长蓝移。当反向偏压达到“吸合偏压”时，上反射镜偏移量达到最大值，谐振波长为 844 nm，此时可实现 16.6 nm 的波长连续调谐。对于 ACD 结构，当外加偏压为 0 时，谐振波长为 850 nm。随着外加偏压的增大，谐振波长蓝移，当外加偏压增大到 28 V 附近时，谐振波长为 830 nm，波长连续调谐范围为 20 nm。进一步增大外加偏压时会发生模式跳变，下一阶纵模处开始激射，波长约为 872 nm，继续增大外加偏压时，波长将继续蓝移，上反射镜偏移量达到最大值时谐振波长蓝移到 852 nm 附近，整体波长调谐范围约为 42 nm。

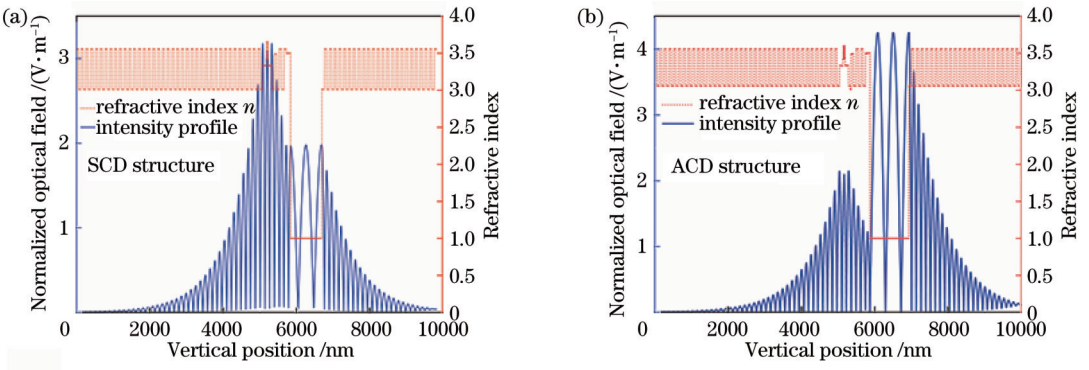

图 7　MEMS-VCSEL 的光场分布。(a) SCD 结构；(b) ACD 结构

Fig. 7　Optical field distribution of MEMS-VCSEL. (a) SCD structure; (b) ACD structure

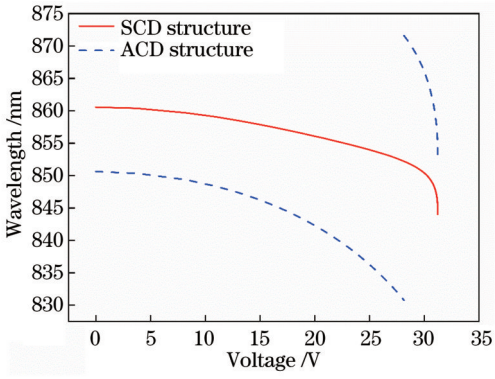

图 8　MEMS-VCSEL 谐振波长随外加偏压的变化

Fig. 8　Resonant wavelength of MEMS-VCSEL varying with applied bias

作为连续扫频光源，MEMS-VCSEL 的谐振频率对光学相干层析成像等扫频应用十分重要，器件本身的谐振频率越高，则调谐速率上限越高，但对于 MEMS 这种偏压谐振器，其外加偏压的升高会显著降低谐振频率。计算了外加偏压从 0 增加到 25 V 时，两种结构的器件的谐振频率，结果如图 9 所示。可以看出：当外加偏压为 0 时，传统等截面结构的固有谐振频率为 195.6 kHz，而双曲线结构的固有谐振频率为 211.1 kHz；随着外加偏压的增大，两种结构的谐振频率均不断降低，但双曲线结构的谐振频率始终高于传统等截面结构，说明优化后结构的调谐特性有所提高。

4　结　　论

针对 MEMS-VCSEL，分析了传统等截面梁结构的应力集中问题，提出了一种双曲线优化方式。通过将支撑梁优化为双曲线结构，增大了支撑梁端面的面积，提升了端面模量，降低了端面应力，使得支撑梁结构上的应力分布更加均匀。理论计算结果表明，优化后支撑梁结构上下表面的最大应力分别降低了 23.4% 和 17%，谐振频率提高了 7.9%，器件的输出特性和可靠性获得了提升。相较于额外封装等其他优化方式，该优化方式工艺简单，兼容性良好，具有一定的应用优势。

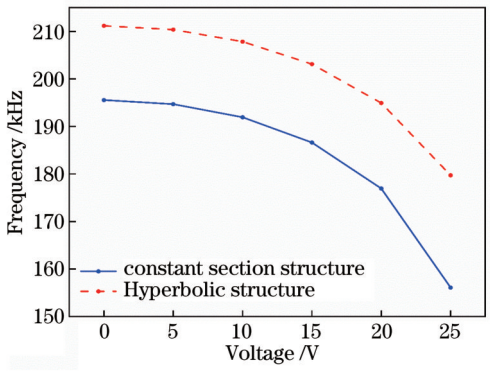

图 9 等截面结构和双曲线结构的谐振频率随外加偏压的变化

Fig. 9 Resonant frequencies of constant section structure and hyperbolic structure varying with applied bias

参 考 文 献

[1] Xie Y Y, Kan Q, Xu C, et al. Low threshold current single-fundamental-mode photonic crystal VCSELs[J]. IEEE Photonics Technology Letters, 2012, 24(6): 464-466.

[2] Jäger R, Grabherr M, Jung C, et al. 57% wallplug efficiency oxide-confined 850 nm wavelength GaAs VCSELs[J]. Electronics Letters, 1997, 33(4): 330-331.

[3] Liu A J, Bimberg D. Vertical-cavity surface-emitting lasers with nanostructures for optical interconnects[J]. Frontiers of Optoelectronics, 2016, 9(2): 249-258.

[4] 王翔媛, 崔碧峰, 李彩芳, 等. 垂直腔面发射激光器横模控制方法的研究进展[J]. 激光与光电子学进展, 2021, 58(7): 0700008.
Wang X Y, Cui B F, Li C F, et al. Research progress of transverse mode control for vertical cavity surface emitting lasers [J]. Laser & Optoelectronics Progress, 2021, 58(7): 0700008.

[5] 陈洋, 王伟. 基于寄生网络的垂直腔面发射激光器频响特性[J]. 激光与光电子学进展, 2022, 59(5): 0514005
Chen Y, Wang W. Frequency response characteristics of vertical-cavity surface-emitting lasers based on parasitic network [J]. Laser & Optoelectronics Progress, 2022, 59(5): 0514005.

[6] 庞海越, 李沼云, 刘欢, 等. 500 GHz宽带双偏振光学频率梳的产生[J]. 中国激光, 2021, 48(9): 0901003.
Pang H Y, Li Z Y, Li H, et al. Generation of 500-GHz broadband dual-polarization optical frequency comb[J]. Chinese Journal of Lasers, 2021, 48(9): 0901003.

[7] Rao M K C, Priya M S, Meenakshi M. MEMS-based multiwavelength tunable 2 × 2 VCSEL array for WDM applications[C]//2012 International Conference on Optical Engineering (ICOE), July 26-28, 2012, Belgaum, India. New York: IEEE Press, 2012.

[8] Chase C, Rao Y, Huang M, et al. 1550-nm wavelength-tunable HCG VCSELs[J]. Proceedings of SPIE, 2014, 8995: 89950A.

[9] Jatta S, Kogel B, Maute M, et al. Bulk-micromachined VCSEL at 1.55 μm with 76-nm single-mode continuous tuning range[J]. IEEE Photonics Technology Letters, 2009, 21(24): 1822-1824.

[10] John D D, Burgner C B, Potsaid B, et al. Wideband electrically-pumped 1050 nm MEMS-tunable VCSEL for ophthalmic imaging[J]. Journal of Lightwave Technology, 2015, 33(16): 3461-3468.

[11] Sahoo H K, Ansbæk T, Ottaviano L, et al. Tunable MEMS VCSEL on silicon substrate[J]. IEEE Journal of Selected Topics in Quantum Electronics, 2019, 25(6): 1700707.

[12] Sahoo H K, Ansbæk T, Ottaviano L, et al. Wavelength tunable MEMS VCSELs for OCT imaging[J]. Proceedings of SPIE, 2018, 10552: 105520I.

[13] Behroozpour B, Quack N, Sandborn P, et al. Method for increasing the operating distance of MEMS LIDAR beyond Brownian noise limitation[C]//CLEO: Applications and Technology 2014, June 8-13, 2014, San Jose, California, USA. Washington, D.C.: OSA, 2014: AW3H.2.

[14] Wu M S, Vail E C, Li G S, et al. Tunable micromachined vertical cavity surface emitting lasers[J]. Electronics Letters, 1995, 31(19): 1671-1672.

[15] Huang M C Y, Zhou Y, Chang-Hasnain C J. A nanoelectromechanical tunable laser[J]. Nature Photonics, 2008, 2(3): 180-184. [LinkOut]

[16] Qiao P F, Cook K T, Qi J P, et al. Wide, continuously swept VCSEL using a novel air-cavity-dominant design[C]//Optical Fiber Communication Conference, March 11-15, 2018, San Diego, California. Washington, D.C.: OSA, 2018: Th1I.7.

[17] Gierl C, Gründl T, Zogal K, et al. Surface micromachined MEMS-tunable VCSELs with wide and fast wavelength tuning [J]. Electronics Letters, 2011, 47(22): 1243-1244.

[18] Inoue S, Nishimura S, Nakahama M, et al. High speed wavelength tuning of MEMS VCSEL with advanced voltage drive technique[C]//2018 IEEE International Semiconductor Laser Conference, September 16-19, 2018, Santa Fe, NM, USA. New York: IEEE Press, 2018: 211-212.

[19] Qiao P F, Li K, Cook K T, et al. MEMS-tunable VCSELs using 2D high-contrast gratings[J]. Optics Letters, 2017, 42(4): 823-826.

[20] Haglund E, Gustavsson J S, Bengtsson J, et al. Demonstration of post-growth wavelength setting of VCSELs using high-contrast gratings[J]. Optics Express, 2016, 24(3): 1999-2005.

[21] Hu Y, Shen X J, Zhang Y Y, et al. Research reviews and prospects of MEMS reliability[J]. Integrated Ferroelectrics, 2014, 152(1): 8-21.

[22] 张文明, 孟光. MEMS可靠性与失效分析[J]. 机械强度, 2005, 27(6): 855-859.
Zhang W M, Meng G. Reliability of MEMS and its failure analysis[J]. Journal of Mechanical Strength, 2005, 27(6): 855-859.

[23] Stanimirović Z, Stanimirović I. Mechanical characterization of MEMS materials[C]//2012 28th International Conference on Microelectronics Proceedings, May 13-16, 2012, Nis, Serbia. New York: IEEE Press, 2012: 177-179.

[24] Tilmans H A C, De Coster J, Helin P, et al. MEMS packaging and reliability: an undividable couple[J]. Microelectronics Reliability, 2012, 52(9/10): 2228-2234.

[25] Tadigadapa S, Najafi N. Reliability of micro-electro-mechanical systems (MEMS) [J]. Proceedings of SPIE, 2001, 4558: 197-205.

[26] Batra R C, Porfiri M, Spinello D. Review of modeling electrostatically actuated microelectromechanical systems[J]. Smart Materials and Structures, 2007, 16(6): R23-R31.

[27] Muvdi B B, Elhouar S. Mechanics of materials[M]. London: Taylor & Francis, 2015.

[28] Tingzon P M, Husay H A, Cabello N I, et al. Indirect stress and air-cavity displacement measurement of MEMS tunable VCSELs via micro-Raman and micro-photoluminescence spectroscopy[J]. Semiconductor Science and Technology, 2022, 37(3): 035013.

[29] Levinshteĭn M, Rumyantsev S, Shur M. Handbook series on semiconductor parameters[M]. Singapore: World Scientific, 1996.

[30] Gupta R K. Electrostatic pull-in test structure design for *in situ* mechanical property measurements of microelectromechanical systems (MEMS)[M]. Cambridge: The MIT Press, 1997.

[31] Qiao P F, Cook K T, Li K, et al. Wavelength-swept VCSELs [J]. IEEE Journal of Selected Topics in Quantum Electronics, 2017, 23(6): 1700516.

[32] Adachi S. GaAs, AlAs, and $Al_xGa_{1-x}As$: material parameters for use in research and device applications[J]. Journal of Applied Physics, 1985, 58(3): R1-R29.

[33] Qiao P F, Su G L, Rao Y, et al. Comprehensive model of 1550 nm MEMS-tunable high-contrast-grating VCSELs[J]. Optics Express, 2014, 22(7): 8541-8555.

Design Optimization of Mechanical Support Structures in Tunable Vertical Cavity Surface Emitting Lasers

Lü Jiagang[1,2], Li Wei[1*], Qi Yuxuan[1,2], Pan Zhipeng[1,2], Zhong Li[1], Liu Suping[1], Ma Xiaoyu[1]

[1]*National Engineering Research Center for Optoelectronic Devices, Institute of Semiconductors, Chinese Academy of Sciences, Beijing* 100083, *China*;

[2]*College of Materials Science and Opto-Electronic Technology, University of Chinese Academy of Sciences, Beijing* 100049, *China*

Abstract

Objective Vertical cavity surface emitting lasers (VCSELs) based on micro-electro-mechanical systems (MEMSs) are widely applied in optical communication, optical coherence tomography, and other fields, with the advantages of wide continuous tuning range, fast tuning rate, and low power consumption. The tuning modes of MEMS-VCSEL include electrostatic, piezoelectric and thermoelectric, but the basic principle is to control the mirror shift to change the overall cavity length of the resonant cavity to achieve wavelength tuning. The support structure of the suspended mirror will be subjected to alternating loads during tuning, and the stress concentration will occur at the fixed end position of the structure, leading to the fatigue fracture. The optimization design of the beam structure can improve the reliability of the device at a low cost, which is a high-feasibility optimization method. In this paper, the support beam structure of the suspended mirror is optimized on the micro/nano-scale, and the hyperbolic beam structure is proposed. The maximum stress is reduced, and the resonant frequency is improved without changing the maximum offset and the corresponding bias of the mirror in the MEMS structure. The proposed optimization method can improve the mechanical and tuning characteristics of the device without introducing additional process steps, which is well compatible with other materials and structure optimization methods.

Methods A hyperbolic beam structure is designed for 850 nm tunable VCSEL based on MEMS to improve the mechanical and tuning characteristics. First, the Mises stress distribution of the traditional constant cross section (CCS) beam structure is analyzed by the finite-element method. The stress concentration problem will appear at the fixed end surfaces because the section modulus at different positions of the structure is the same with different moments when the CCS beam structure is subjected to uniform load. Then, the maximum stress on the structure can be reduced by increasing the geometry size of the end surface, and the stress distribution can be more uniform. Based on this theory, the hyperbolic beam structure is designed. In addition, the maximum offsets of the two structures before and after optimization are compared, which means that the stress optimization results do not sacrifice the offset of the mirror. Finally, the relationship between the resonant wavelength of MEMS-VCSEL and the applied bias is calculated by the frequency domain analysis method, and the resonant frequencies of the MEMS structure before and after optimization are compared.

Results and Discussions The mechanical and tuning characteristics of the two structure beams before and after optimization are compared. The most important parameters of mechanical properties are the maximum stress and offset of the structure. The stress distribution of the traditional CCS beam structure and the hyperbolic beam structure is calculated when the offset is 390 nm. As shown in Figs. 4 and 5, the stress distribution of the two structures is similar. For the traditional CCS beam structure, the maximum stress values of the upper and lower surfaces are 3.25×10^7 and 3.06×10^7, respectively. For the hyperbolic beam structure, the values are 2.49×10^7 and 2.54×10^7 respectively, which indicates that the maximum stress is reduced by 23.4% and 17.0% after optimization. For hyperbolic beam structure, hyperbolic shapes and stress reduction effects are both different, which means that the best mechanical properties can be obtained by optimizing the size of the hyperbolic beam structure. The wavelength tuning range and tuning rate are the most important parameters to evaluate the tuning characteristics of tunable lasers. The relationship between the offset of the upper mirror and the applied bias in the MEMS structure is calculated, and then the relationship between the cavity length of the laser and the applied bias is obtained. The wavelength tuning range of the device is obtained by the frequency domain analysis

method, and the results are shown in Fig. 8. The influence of the air gap on the resonant wavelength is different under different coupling modes of the semiconductor cavity and the air cavity in the laser. For the semiconductor-cavity dominated (SCD) structure, the wavelength tuning range is narrow (16.6 nm), but it is continuously tuned in the whole range. For the air-cavity dominated (ACD) structures, the wavelength coverage is 42 nm, but "mode hopping" occurs during tuning. The resonant frequencies of the two beam structures will decrease with the increasing applied bias, but the resonant frequency of the hyperbolic beam structure is always increased by 7.9% compared with the CCS beam structure.

Conclusions A hyperbolic beam structure is designed to improve the mechanical and tuning characteristics of MEMS-VCSEL devices. The main principle is to reduce the maximum stress and improve the elastic coefficient of the structure by increasing the section size of the large bending moment. The maximum stress of the upper and lower surfaces decreases by 23.4% and 17.0% after optimization when the offset is 390 nm. There is little difference between the two structures in the maximum offset and the required applied bias. In addition, the resonant frequency of the hyperbolic beam structure is increased by 7.9%. The wavelength continuous tuning range is 16.6 nm when the coupling structure between the two cavities in the laser is SCD structure. The wavelength coverage is about 42 nm for the ACD structure, but there is a "mode hopping" phenomenon during tuning. This optimization method does not need to change the structure of the laser, and is compatible with other optimization methods, with certain application prospects.

Key words lasers; vertical cavity surface emitting lasers; tunable lasers; micro-electro-mechanical system; mechanical characteristic; tuning characteristic